COBRAMSEG 2014
9 a 13 de setembro de 2014 - Goiânia/GO - Brasil
XVII Congresso Brasileiro de Mecânica dos Solos e Engenharia Geotécnica
VII Congresso Luso-Brasileiro de Geotecnia
VI Simpósio Brasileiro de Mecânica das Rochas
VI Simpósio Brasileiro de Jovens Geotécnicos

# Numerical analysis of the performance of excavator buckets for dry granular media

Davi S Barreira
Universidade Federal do Ceará, Fortaleza, Brazil, davisbarreira@gmail.com

Sergio Galindo-Torres
The University of Queensland, Brisbane, Australia, s.galindotorres@uq.edu.au

Dorival M Pedroso
The University of Queensland, Brisbane, Australia, d.pedroso@uq.edu.au

SUMMARY: The understanding of soil-tool interaction is of fundamental importance for improving the efficiency during earth-works. The digging process using excavator buckets is perhaps the most common example of soil-tool interaction. This paper presents complete numerical analyses via the Discrete Element Method of these types of interactions. The analyses are validated against some experimental data and other numerical results showing good representative capabilities. A series of simulations are performed, comparing both bucket geometry and soil properties. An evaluation of the excavation performance is conducted in terms of energy expenditure per volume of soil excavated. Our results show that the presence of teeth in the bucket causes some improvement on the efficiency when handling cohesive soils but to a lesser extent when excavating cohesionless fragments. Results are also presented for simulations with different grain size distributions, in addition to discussions of the effect of wearing on the excavator tool.

KEYWORDS: DEM, excavation, energy efficiency, numerical modeling.

## 1 INTRODUCTION

The process of earthmoving plays a major role in several engineering activities, such as mining, agriculture and construction. The increase of efficiency on this process is then highly desirable not only economically, but also to the benefit of the environment (Tsuji et al, 2012). The key characteristic to achieve these two goals is the reduction of fuel expenditure. To this end, the optimization of machinery design can be taken as an essential step.

In geomechanics, excavator buckets are largely used in earthmoving works. For instance, they are present in several hydraulic excavators, shovels, loaders and draglines. Understanding the interaction of buckets with granular material is of interest to achieve an economic and environmental friendly design. Nonetheless, this is hard to be directly assessed by fundamental means due to the great complexity of the micro/mesoscopic mechanisms involved. Examples of complex configurations include particles with different shapes and varied sizes.

Improvements in design can be made by running experiments at real scale with field measurements, although such methods are often expensive which makes them unfeasible especially when considering several designs for a number of different soils (Coetzee et al, 2007). Numerical simulation can then be employed to this purpose, as long as they are previously calibrated. The Discrete Element Method (DEM) is a numerical tool with the potential to answer these questions. The DEM was introduced by Cundall and Strack (1979) and stands out among other tools due to its capabilities of analyzing microscopic aspects such as the internal forces in a porous media. The DEM can also be used to the modeling of fractions and segregation of material during excavations.

The process of excavation with buckets has

been previously addressed in the literature with DEM models, usually showing good qualitative results when compared with experimental data as presented in the works of Coetzee et al (2009) and Obermayr et al (2013). However, quantitative results still lack precision, fact that may be partially attributed to difficulties in calibrating the microscopic parameters which cannot be obtained from experiments that only allow observing and measuring the macroscopic response. For instance, the works of Obermayer et al (2013) and Coetzee and Els (2009) compared DEM simulations with experimental results and found that the technique is capable of reproducing the soil response but not always reproduced the quantitative estimate for draft forces (Coetzee et al, 2009). On other works, Tsuji *et al* (2012) have used DEM for modeling the interaction of cohesive soil with a bulldozer and Wu *et al* (2013) have shown how the DEM can be useful for optimizing the structure design in cutterhead systems of earth pressure balance (EPB) machines.

In this paper, a three-dimensional DEM simulation tool is used to study the process of excavating soils using excavator buckets. Several simulations are performed to study the effects of bucket teeth and soil properties in the process. The results are qualitatively validated against results found in the literature. The energy efficiency of the system is carefully evaluated based on the resisting forces acting on the bucket per volume excavated. Finally, the forces along a cross section of the bucket surface are analyzed, providing some insight on possible wearing prone regions and giving indication on how to prevent this problem.

## 2 DISCRETE ELEMENT MODELLING

Since the work by Cundall and Strack (1979), the use of the Discrete Element Method (DEM) to simulations of granular assemblies has grown with a number of papers being published on the topic (H.P, Zhu et al, 2007). The DEM is a different modelling approach when compared to conventional methods such as the ones based on continuum mechanics like the Finite Element Method (FEM) because it considers the mechanical behaviour of each particle and their interactions. In this way, the macroscopic response observed experimentally can be reproduced (see e.g. C. O'Sullivan, 2011). In the DEM, particle's interactions are governed by Newton's equation of motion assuming a string, a dashpot and a slider component at the contact (Zhang and Whiten, 1996). The model allows the calculation of reaction forces when particles overlap, which can be interpreted as the particles deformation. Figure 1 illustrates the interaction between two particles and some of the parameters used in the calculation of the reaction forces.

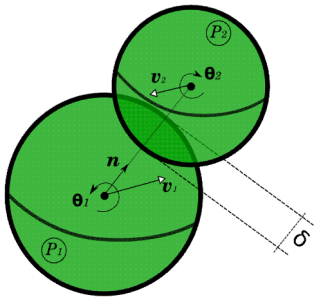


Figure 1. DEM Particles Interaction.

Considering two particles namely P1 and P2, with respective radius *R1* and *R2*, the overlap between them in a specific time-step can be calculated as

$$\delta_{12} = R1 + R2 - || \boldsymbol{x}_1 - \boldsymbol{x}_2 || \quad (1)$$

Where $\boldsymbol{x}_1$ and $\boldsymbol{x}_2$ represent the Cartesian coordinates of the particles in a 3D plane. In a similar manner, a normal vector $\boldsymbol{n}$ may be calculated by:

$$\boldsymbol{n}(P_1, P_2) = \frac{(\boldsymbol{x}_1 - \boldsymbol{x}_2)}{|| \boldsymbol{x}_1 - \boldsymbol{x}_2 ||} \quad (2)$$

Therefore, the normal reaction force between the collisions of the particles is given by:

$$\boldsymbol{F}_n(P_1, P_2) = K_n \boldsymbol{n}(P_1, P_2)\delta_{12} \quad (3)$$

Where K*n* *is* the normal stiffness coefficient. The particles contact has also a tangential component from which the deformation ξ can be calculated as follows:

$$\boldsymbol{\xi}_{12} = \{(\boldsymbol{v}_1 - \boldsymbol{v}_2) - ((\boldsymbol{v}_1 - \boldsymbol{v}_2)\cdot \boldsymbol{n})\boldsymbol{n} - (\boldsymbol{\theta}_1 R_1 + \boldsymbol{\theta}_2 R_2)\times \boldsymbol{n}\}\Delta t \quad (4)$$

Where the $\boldsymbol{v}$ is the linear and $\boldsymbol{\theta}$ the angular velocity of each particle. Therefore, after knowing $\xi_{12}$, the friction force (tangential force) can be calculated by

$$\boldsymbol{F}_t(P_1, P_2) = K_t \boldsymbol{\xi}_{12} \quad (5)$$

The friction force is limited by the Coulomb-type friction law, meaning that the shear force can only grow until a maximum value for $F_t > F_n \mu$. When such limit is reached the force goes to $\boldsymbol{F}_t = F_n \mu \boldsymbol{\xi}/\xi$ (Galindo-Torres et al, 2012).

The damping component is given by viscous forces, which are added to account for the gain of energy in the system as described Eq 6. The viscous coefficient, relative velocity component and the effective mass of the particles pair are $G$, $\boldsymbol{V}$ and $m_e$ respectively. The "n" and "t" indices represent the normal and tangential components (Galindo-Torres et al, 2012).

$$\boldsymbol{F}_v = G_n m_e \boldsymbol{V}_n + G_t m_e \boldsymbol{V}_t \quad (6)$$

After obtaining the total force acting on the particle, a Leapfrog scheme is used to solve the Newton's equation of motion and the angular dynamical equations (Wang et al, 2006).

Other forces can also be incorporated in the DEM code for simulating processes such as cohesion. For this paper, a simple cohesion model was implemented based on the work of Luding (2008) using a variant of the hysteretic spring model with constant stiffness coefficients.

## 3 MODEL SETUP

A three-dimensional DEM model is used for simulating the excavation process with a bucket digging out soil in a semi-circular trajectory as illustrated in Fig. 2. The geometry of the simulation has a radius of 3.20 m and the bucket is initially set with a linear velocity of 0.41 m/s. The trajectory is illustrated in Fig 2. The soil particles are represented as spheres and rolling resistance is added to account for excessive rolling caused by the spherical shape and in such a way introduce the effect of a more general shape for the grains.

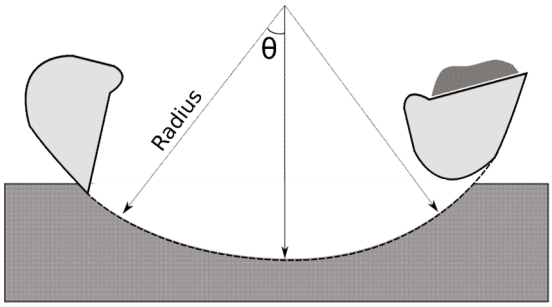


Figure 2. Excavation Trajectory.

Two excavator bucket designs are considered in this work: with and without teeth. Comparisons in terms of energy performance are then carried out. Due to the complex geometry of the buckets, the soil-tool interaction may give rise to singularities in the calculations, e.g when particles interact with the sharp edges of the bucket teeth. To avoid such issues a spheropolyhedra approach is adopted. Such technique allows a more efficient definition of the contact laws for particles with complex geometry by smoothing edges and sharp vertices, without much interference in the overall shape of the particle (Galindo-Torres and Pedroso, 2010). The use of spheropolyhedra consists in sweeping a sphere around the element of distinct geometry as illustrated in Fig 3 (Galindo-Torres and Pedroso, 2010). The contact laws are then reduced to the more simplified sphere-to-sphere contact law avoiding singularities (Fig 4).

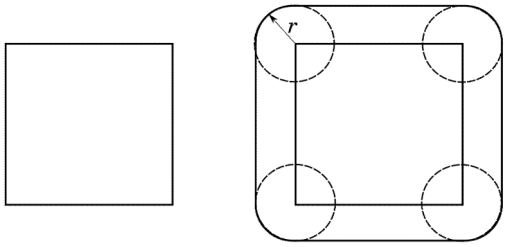


Figure 3. Spheropolyhedra applied to square particle with a radius r.

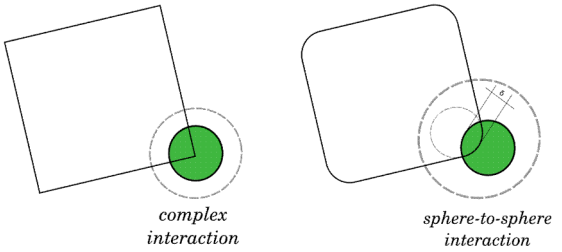


Figure 4. Contact laws simplification with spheropolyhedra.

The choice of the proper radius for smoothing the bucket must be small enough to not alter significantly the soil-tool interaction, but large enough to avoid excessive particle overlap. The value used was of 1 cm. The bucket with teeth is shown in Fig. 5. comparing the shapes before and after the polygon dilation applying a radius of 1cm.

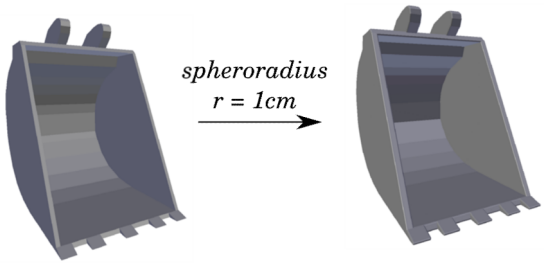


Figure 5. Comparison of bucket with teeth with and without applied sphero-radius.

## 3.1 Particles with Cohesion

Simulations are performed with and without cohesive forces. A simple approach for calculating such forces is implemented using a variation of the linear spring model. This novel approach was introduced by Luding (2008) as a simplified version of the nonlinear-hysteretic force laws. The model requires the addition of two stiffness parameters representing the unloading and minimum plastic forces, namely $B_n$ and $B_t$. The use of these two parameters together with the usual $K_n$ form a triangular surface which represents the possible hysteretic forces ($Fh$) during particles contact, as seen in Fig 7.

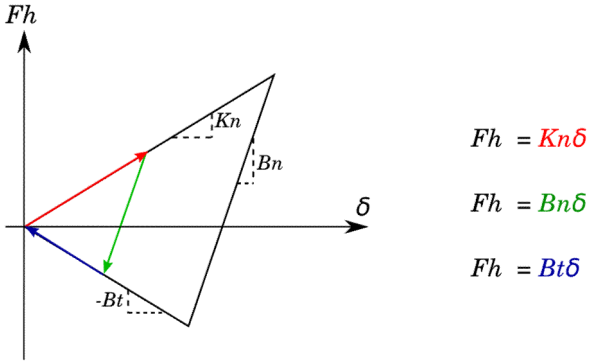


Figure 6. Cohesion Model (mod. from Luding, 2008)

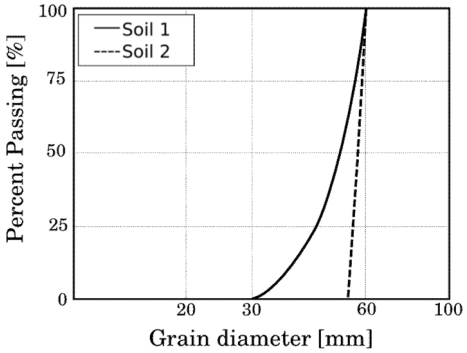


Figure 7. Grain size distribution of the two sets of soils used in the numerical simulation

The triangular diagram can be better explained as different phases of particles interaction. The first phase consists of an initial overlap representing compression of the granular material, highlighted by the red arrow in Fig 7. In this stage, the force is repulsive and follows a slope $K_n$ as shown in the cohesionless model. Secondly, the particles start to move apart, making the contact force decrease along the green line with $B_n$ slope until a minimum value limited by the a line of slope $B_t$, this would be called an unloading phase. After the force reaches its minimum value, as the overlap decreases the force follows the blue arrow. When $Fh$ becomes negative, the attraction force is predominant over the repulsive force, simulating the cohesion process between the particles. The goal behind this simplified model is the simulation of the path-dependence of elasto-plastic soil behavior.

### 3.2 Soil Assemblies and Grain Size Distributions

Two sets of soils assemblies with different grain size distributions are investigated. The distributions are presented in Fig 6. Both sets are generated with coarse particles and one of them (indicated by Gradation Soil 2) has a more homogeneous distribution. Table 1 presents the parameters used for each assembly.

Table 1. Soil properties.

| Parameters | | Soil 1 | Soil 2 |
|---|---|---|---|
| Maximum Diameter (mm) | *Dmax* | 60 | 60 |
| Minumum Diameter (mm) | *Dmin* | 30 | 54 |
| Normal Stiffness(N/m) | *Kn* | 3.50E+05 | 3.50E+05 |
| Tangential Stiffness (N/m) | *Kt* | 1.00E+05 | 1.00E+05 |
| Friction coefficient | $\mu$ | 0.34 | 0.34 |
| Porosity | $\eta$ | 0.47 | 0.47 |
| Cohesive Stiffness Parameters (N/m) | *Bn, Bt* | 5.00E+05 | 5.00E+05 |
| Coefficient of curvature | *Cc* | 1.11 | 1.08 |
| Coefficient of uniformity | *Cu* | 1.56 | 1.51 |
| Dumping coefficient ($s^{-1}$) | *G* | -0.2 | -0.2 |

## 4 RESULTS AND DISCUSSION

Several simulations are performed with many combinations of geometries and properties. Table 2 collects information on these simulations and introduces a system of keys to make the analysis easier.

Table 2. List of all simulations performed.

| Id | Soil Type | Bucket Geometry | Cohesion |
|---|---|---|---|
| 1 | 1 | Teeth | No |
| 2 | 1 | No teeth | No |
| 3 | 2 | Teeth | No |
| 4 | 2 | No teeth | No |
| 5 | 2 | Teeth | Yes |
| 6 | 2 | No teeth | Yes |

### 4.1 Model Validation

The reaction forces obtained in all simulations exhibit very similar trends as observed in Fig 8a and Fig 8b. A comparison with the experimental results of Obermayer et al (2013) serves as a qualitative validation of the model and is given in Fig 9a and Fig 9b. Two fundamental differences can be found between our results and their results nonetheless. In our results the horizontal force component does not go to zero at the end of the simulation, and the vertical force (z-axis) does not quite stabilize. The reason for this is due to the fact that the defined trajectory of the bucket does not account for the stopping of motion – the trajectory is set to complete the semi-circle with constant velocity and is ceased before the forces can settle when the bucket stops. If the trajectory accounted for such stopping motion and the simulation was ran for a longer time the forces would eventually stabilize as observed in numerical simulations involving less particles. Figure 10 illustrates the simulation for one of the simulated scenarios.

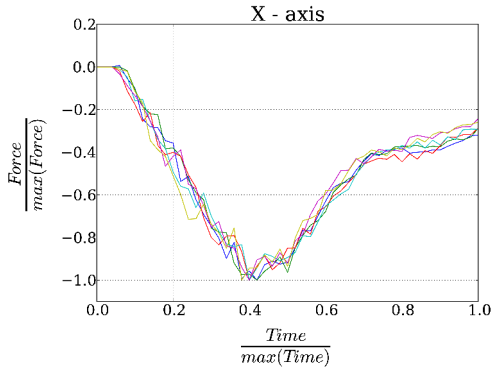


Figure 8a. Horizontal force acting on the excavator bucket for different simulations.

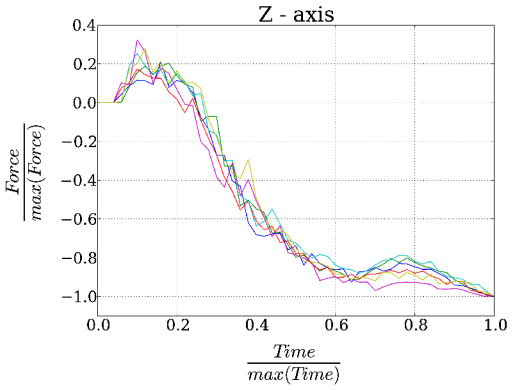


Figure 8b. Vertical forces acting on the excavator bucket for different simulations.

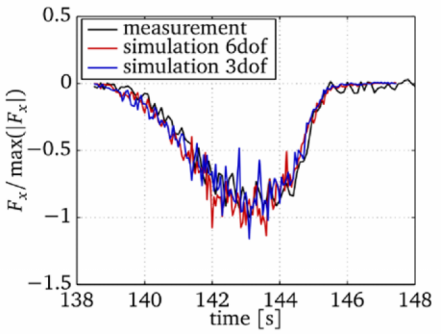


Figure 9a. Horizontal force acting on bucket, for experimental and DEM simulation results. From Obermayr et al, 2013.

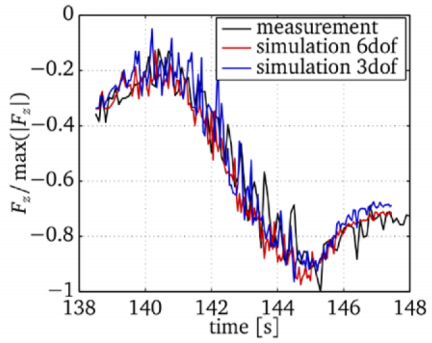


Figure 9b. Vertical force acting on bucket, for experimental and DEM simulation results. From Obermayr et al, 2013.

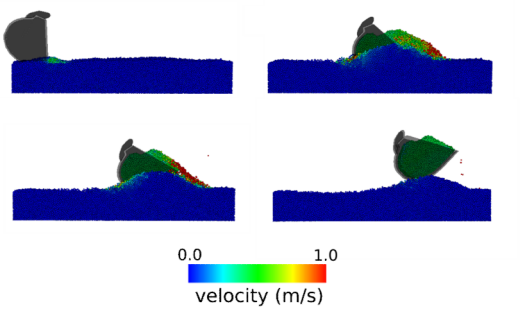


Figure 10. Excavation of Soil Simulation

## 4.2 Excavation Results

With the reaction forces acting on the bucket and the predefined trajectory, the work (or energy) used for the excavation cycle is calculated by integrating over each time-step of the simulation.

The number of particles excavated in each simulation is used to estimate the volume dug in each scenario. This can be easily calculated since all particles are spherical and with known radius. Figure 11 presents a summary of the excavation results.

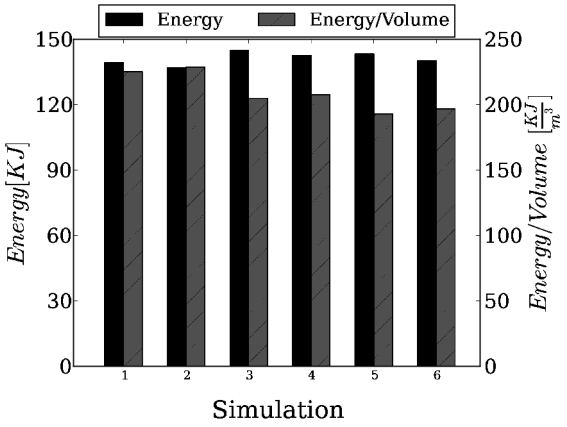


Figure 11. Simulation Results.

## 4.3 Bucket Design Efficiency

The effect of teeth in the bucket is compared for three different scenarios: (1) with cohesionless soil of type 1; (2) with cohesionless soil of type 2; and (3) with cohesive soil of type 2. It is observed that the presence of the teeth does not have a great effect in reducing the spent energy; on the contrary, the teeth caused increase of the energy expenditure in the order of 1%. This result is actually similar with the findings by Maciejewski et al (2003) on real experiments. It is worth noting that, for practical matters, the consideration of energy expenditure alone is not the best strategy to evaluate the global efficiency of the global excavation phenomenon. A better parameter is the energy expenditure divided by the excavated volume, since more excavated volume leads invariably to more work done by the excavator bucket as it lifts more weight. With this normalized quantity, the teeth actually show a reduction on energy of 2.0% when excavating cohesive soils and an average of only 1.4% when excavating cohesionless soils. As can be seen in Table 3, all three scenarios the bucket with teeth outperformed the bucket without teeth in terms of energy per volume. It is important to notice that the performance consideration in terms of cohesive soil must be taken with caution as different soils have different cohesion aspects

which may affect the efficiency.

Table 3. Comparison of Bucket Geometry Efficiency. In the properties the "NC" stands for cohesionless soil and the "C" is for cohesive.

| Simulation | Ratio of Energy Increase | Ratio of Energy/Volume Increase | Properties |
|---|---|---|---|
| 1 – 2 | 1.68% | -1.6% | Soil 1 – NC |
| 3 – 4 | 1.57% | -1.3% | Soil 2 – NC |
| 5 – 6 | 2.21% | -2.0% | Soil 2 – C |

## 4.4 Particle Size Distribution Effects

When comparing the two sets of particles with different particle size distributions, it is observed that the more homogeneous (soil type 2) required less energy per volume during excavation than when excavating the one with a better graded distribution. Again this shows how the sole evaluation of efficiency considering only energy can be misleading. The effect of the gradation was considerable, even more then the bucket geometry, presenting an improvement in efficiency of the order of 9% for the more homogeneous soil as shown in Table 4.

Table 4. Comparison of Soil Efficiency.

| Simulation | Ratio of Energy Increase | Ratio of Energy/Volume Increase | Properties |
|---|---|---|---|
| 1 – 3 | -4.07% | 9.1% | No Teeth |
| 2 – 4 | -4.19% | 9.3% | Teeth |

## 4.5 Stresses Acting on the Bucket Surface

During the excavation process, the particles hit the bucket and may damage it. Numerical models such as the DEM enable the mapping of both normal and tangential stresses acting around a body. The stresses acting on the bucket surface was then analyzed for some of the buckets at given time during the simulation. Fig. 12 presents the diagrams of the stresses acting across the bucket profile.

The particles friction force acting on the bucket may lead to material erosion (wear), which is one of the main causes related to machinery fail (see, e.g. Popov, 272). Therefore the knowledge regarding probable wear-conditioned regions is of high interest of engineers when designing machinery.

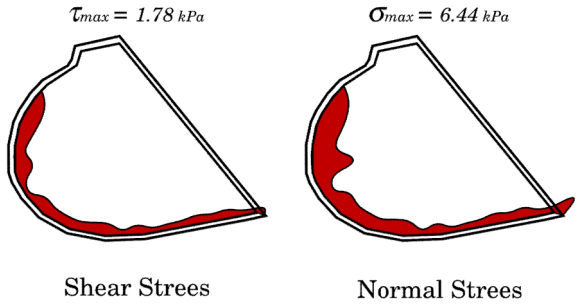


Figure 12. Stress distribution across bucket profile at time of 7.5 seconds. The values are given in local coordinates from the bucket surface.

This analysis only considered abrasive wear which occurs due to friction between bodies of different hardness. The volume of wear debris is approximate $W/\sigma_o$ , where $W$ is the frictional work and $\sigma_o$ the material hardness (see, e.g. Popov, 274). Therefore, the wear-conditioned areas are the ones in which the tangential force acting on the bucket reaches the Coulomb-type friction law limit, and can be seen in Fig 13 for the moment the bucket is deeper in the soil.

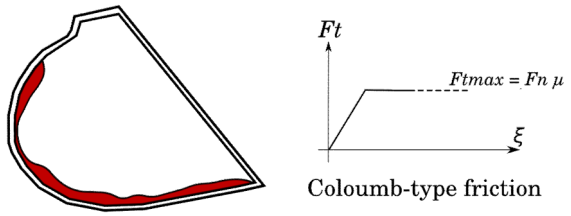


Figure 13. Wear-conditioned area for time of 7.5 seconds and coloumb-type friction law illustration.

## 5 CONCLUSIONS

This paper presented a comprehensive numerical analysis of excavation of dry granular materials. Analyses are conducted with the Discrete Element Method (DEM) which can provide a better insight on the fundamental mechanics of granular media. The results show qualitative similarities with a set of experimental data and are able to reproduce the findings of another set of numerical tests. In particular, the results show that the addition of

teeth at the front edge of the excavator bucket does not decrease the energy expenditure during the filling process. The numerical simulations show that the performance of the bucket with teeth varies from 1.5% for excavation of granular media to 3% for cohesive soils.

With regards to the grain size distribution of the soil assembly, the results show that it is easier to handle more homogeneous soils than heterogeneous ones. For instance, the grain size distribution presented significant impact in terms of efficiency, with 10% of improvement being achieved in more homogeneous soils.

Finally, the discrete element code with the sphero-polyhedra technique is able to provide qualitative results for the prediction of soil-tool interaction, such as the stresses distributions which can be useful for identifying wear-conditioned regions. These results can then be used by the interested industry for optimizing earthworks.

## REFERENCES


Coetzee C.J., Basson A.H., Vermeer P.A. (2007). Discrete and continuum modelling of excavator bucket filling. J Terramech , 44 (2007) 177–186.

Coetzee C.J., Els D.N.J. (2009). The numerical modelling of excavator bucket filling using DEM. J Terramech, 46 (2009) 217–227.

Coetzee C.J., Els D.N.J., Dymond G.G (2009). Discrete element parameter calibration and the modelling of dragline bucket filling. J Terram., 47 (2010) 33–44.

Cundall, P. A.& Strack, O. D. L. (1979). A discrete numerical model for granular assemblies, Geotechnique, 29: 47-65

Galindo-Torres, S. A. & Pedroso, D. M. (2010). Molecular dynamics simulations of complex-shaped particles using Voronoi-based spheropolyhedra. Physical Review E, 81, 061303.

Galindo-Torres, S. A., Pedroso, D. M, Williams D. J, Li L (2012). Breaking processes in three-dimensional bonded granular materials with general shapes. Computer Physics Communications,183(2), 266-277.

Luding, S. Cohesive, frictional powders: contact models for tension (2008). DOI 10.1007/s10035-008-0099-x

Maciejewski, J., Jarzębowski, A., Trąmpczyński, W.: The Influence of Teeth Wear on The Digging Process. In: Proceedings of the 9th European Conference of the ISTVS, Harper Adams, UK, pp. 273–282 (2003)

Obermayr, M., Vrettos, C., Kleinert, J. & Eberhard, P. (2013). A discrete element method for assessing reaction forces in excavation tool.

O'Sullivan, C. & Ebooks Corporation (2011). Particulate discrete element modelling: a geomechanics perspective, Taylor & Francis, London.

Popov, V.L (2010). *Contact Mechanics and Friction*. Germany: Springer Heidelberg. 271-274.

Tsuji T., Nakagawa Y., Matsumoto N., Kadono Y., Takayama T., Tanaka T.. 3-D DEM simulation of cohesive soil-pushing behavior by bulldozer blade. J Terramch 2012, 49 (2012) 37-47.

Wu L., Guan T., Lei L, Discrete element model for performance analysis of cutterhead excavation system of EPB machine, Tunnelling and Underground Space Technology, Volume 37, August 2013, Pages 37-44, ISSN 0886-7798.

Wang Y., Abe S., Latham S., Mora P., Implementation of particle-scale rotation in the 3-D lattice solid model, Pure Appl. Geophys. 163 (9) (2006) 1769–1785.

Zhang D, Whiten WJ. The calculation of contact forces between particles using spring and damping models. Powder Technol 1996;88:59–64.

Zhu, H., Zhou, Z., Yang, R. & Yu, A. (2007). Discrete particle simulation of particulate systems: theoretical developments. Chemical Eng Science, 62, 3378-3396.